Layer-dependent magnetic phase diagram in FenGeTe2 (3≤n≤7) ultrathin films: coexistence of localized and itinerant electronic states of Fe with variable valence

Qinxi Liu
Dalian University of Technology
Jianpei Xing
Dalian University of Technology
Zhou Jiang
Dalian University of Technology
Yu Guo
Dalian University of Technology
Xue Jiang (jiangx@dlut.edu.cn)
Dalian University of Technology
Yan Qi
Dalian Minzu University
Jijun Zhao
Dalian University of Technology

Article

Keywords: magnetic, temperature, ultrathin, films, high

Posted Date: October 25th, 2021

DOI: https://doi.org/10.21203/rs.3.rs-961504/v1

Version of Record: A version of this preprint was published at Communications Physics on June 3rd, 2022. See the published version at https://doi.org/10.1038/s42005-022-00921-3.

Layer-dependent magnetic phase diagram in Fe_nGeTe_2 ($3\leq n\leq 7$) ultrathin films: coexistence of localized and itinerant electronic states of Fe with variable valence

Qinxi Liu [1], Jianpei Xing [1], Zhou Jiang [1], Yu Guo [1], Xue Jiang [1]*, Yan Qi [2,1]*, Jijun Zhao [1]

[1]Key laboratory of Material Modification by Laser, Ion and Electron Beams (Dalian University of Technology), Ministry of Education, Dalian, 116024, China

[2]School of Physics and Materials Engineering, Dalian Minzu University, Dalian 116600, China

Abstract

Two-dimensional (2D) ferromagnets with high Curie temperature (T_C) are highly desirable due to their potential applications in spintronic devices. However, they are rarely obtained in experiments mainly due to the challenge of synthesizing high-quality 2D crystals, and their T_C values are below the room temperature. By first-principles calculations, herein we design a family of stable 2D Fe_nGeTe_2 ($4\leq n\leq 7$) ultrathin films that are similar to the reported Fe_3GeTe_2, which exhibit coexistence of itinerant and localized magnetism. Among them, 2D Fe_3GeTe_2 and Fe_4GeTe_2 are ferromagnetic metals with T_C of 138 K and 68 K, respectively; 2D Fe_5GeTe_2, Fe_6GeTe_2 and Fe_7GeTe_2 ultrathin films are Néel's P-types, R-type, R-type ferrimagnetic metals with T_C of 320 K, 450 K and 570 K, respectively. The thickness induced magnetic phase transition is mainly originated from the competition between itinerant and localized states, which is also correlate well with the content of Fe^{3+} and Fe^{2+} ions. A valence/orbital dependent magnetic exchange model is proposed to clarify such interesting thickness and composition effect. Our results not only endow 2D Fe-Ge-Te ultrathin films as promising candidates for spintronics at room temperature, but also propose a universal mechanism to understand the magnetic coupling in complex magnetic systems.

*Corresponding authors. E-mail: jiangx@dlut.edu.cn (Xue Jiang), qiyan@dlnu.edu.cn (Yan Qi)

Since the successful exfoliation of monolayer CrI_3 and bilayer $CrGeTe_3$ sheets, the family of two-dimensional (2D) magnetic materials have been extraordinarily growing during the past few years. Right now, the range of 2D magnets covers insulators, semiconductors, half-metals, and metals. Among them, the most concerned ones are ferromagnetic (FM) semiconductor, such as CrX_3, NiX_3, $CrGeTe_3$ and RuX_3 (X=Cl, Br and I).[1, 2, 3, 4, 5, 6] Magnetism in these compounds originates from localized *d* electrons and the magnetic ordering is usually mediated by superexchange interaction between the magnetic ions through the non-metal atoms. The semi-empirical Goodenough-Kanamori-Anderson (GKA) rules provide valuable picture to describe the magnetic interactions in these 2D compounds.[7, 8, 9] According to the GKA rules, the ferromagnetism in 2D semiconductors is mainly derived from 90° *d-p-d* superexchange. In this situation, the occupied orbitals overlap with different orthogonal *p* orbitals of a ligand. It is thus not surprising that weak ferromagnetism is usually found in those systems. As representatives, the observed Curie temperatures (T_C) of the 2D compounds of CrI_3 and $CrGeTe_3$ are 45 K and 30 K, respectively, which are far below the room temperature.[1, 4]

Beyond these ferromagnetic semiconductors, metallic ferromagnet is another important member of 2D ferromagnet. A prominent advantage of the metallic ferromagnet is that its metallic nature enables the interplay between spin and charge degrees of freedom, which are the main concern in spintronics.[10] The reported metallic ferromagnets, such as Cr_2BC, $FeSe_2$, FeTe, MnSe and Fe_nGeTe_2, shown robust ferromagnetism with higher T_C (130–846 K).[11, 12, 13, 14, 15, 16, 17, 18, 19] Especially, 2D metallic Fe-Ge-Te ternary compounds (FGT) with high T_C and huge MAE along the c axis have attracted attention. Among the FGT thin films, 2D Fe_3GeTe_2 was first achieved by cleaving Fe_3GeTe_2 bulk crystal onto a gold film evaporated on top of SiO_2/Si substrate. The polar reflective magnetic circular dichroism measurement confirmed that the T_C were preserved at 68−130 K with MAE value of ~2.0 meV at the monolayer limit.[13, 14] Subsequently, Kim *et al.* have successful synthesized and exfoliated Fe_4GeTe_2 flakes and the T_C for a seven-layer Fe_4GeTe_2 system of 7 nm thickness was determined to be about 270 K. However, the observed MAE reduces from 1.03 to 0.23 J/cm^3 when the composition changes from Fe_3GeTe_2 to Fe_4GeTe_2.[15] Another important member of FGT system is $Fe_{5-x}GeTe_2$, May *et al.* fabricated FM $Fe_{5-x}GeTe_2$ nanoflakes with higher T_C of 270–310 K by mechanically exfoliated method.[16]

So far, spontaneous magnetization in most of 2D metallic ferromagnet is generally accepted to be the itinerant electrons, which can be understood by the well-known Stoner model.[20] The electrons behave ferromagnetic just because of their repulsive Coulomb interaction, while the contributions from lattice and band structure are totally ignored. Beneficial from the delocalized electrons, the reported metallic ferromagnets in most cases shown higher T_C than ferromagnetic semiconductors. However, lots of works suggested that metallic FGT systems is not conventional Stoner ferromagnets. The itinerant magnetism could not totally explain the variation of T_C in FGT systems. For example, Dai *et al.* founded that the increased hydrostatic pressure lead to the enhancement of electron itinerancy but decreased the T_C in thin Fe_3GeTe_2 flakes.[21] Yang *et al.* noticed that the band dispersions of Fe_3GeTe_2 barely change upon heating towards the ferromagnetic transition near 225 K, which also strongly deviates from itinerant Stoner model.[22] Deng *et al* used localized Heisenberg model to properly estimate the magnetic properties in 2D Fe_3GeTe_2, which consistent with the experiment results.[14] All these results suggest that the local magnetic moments may play a crucial role in the ferromagnetic ordering of Fe-Ge-Te systems. From above experimental reports, we can conclude that 2D metallic FGT are prospective candidates for room-temperature ferromagnet. However, there still exist several unsolved issues, such as the physical origin of their localized magnetism in metallic systems, the validity of Stoner model and Heisenberg model, the effect of composition/thickness, and the influence of magnetic anisotropy.

To reveal these issues, the electronic and magnetic properties of 2D Fe_3GeTe_2 were systemically investigated in this work. We found that the five 3*d* orbitals of 2D Fe_3GeTe_2 could divide into two parts, a_1 (d_{z2}) states mostly localized on the Fe sites and give rise to local spin moments, while the other e_1 (d_{xy}/d_{x2-y2}) and e_2 (d_{xz}/d_{yz}) states are itinerant. According to the orbital occupation behavior of localized a_1 (d_{z2}) states and coordination environments, the final valence states for Fe atoms in Fe_3GeTe_2 can been classified into +2 and +3. For localized spins on Fe atoms, we propose a valence-dependent multipath magnetic coupling mechanism to describe the competition between the interlayer ferromagnetism and antiferromagnetism, while itinerant e_1 and e_2 states always favor in intra- and interlayer ferromagnetism in 2D Fe_3GeTe_2. Furthermore, the MAE also depended on the valence state of Fe ions, which origin from the coupling between a_1 and e_2 states. Based on these findings, we further construct a series of 2D

Fe_nGeTe_2 ultrathin films ($4 \leq n \leq 7$) with different Fe contents and thicknesses. Their combined effect on magnetic moment, magnetic exchange parameters, and MAE has been discussed. We found the value of T_C in Fe_nGeTe_2 ultrathin films is indeed depended on the competition between the localization and itinerant magnetism. An interesting thickness-induced magnetic phase transformation from ferromagnets to Néel's P-types ferrimagnets, and then to R-type ferrimagnets are observed in 2D Fe_nGeTe_2 films, and their T_C are in the range of 68−570 K. Our results not only reveal a new way to design 2D intrinsic magnets with high Curie temperature but also provide a universal theoretical model for analyzing the itinerant and localized magnetism in complex materials.

Results

Co-existence of localized and itinerant magnetism in 2D Fe_3GeTe_2. The atomic configuration of 2D Fe_3GeTe_2 is shown in **Fig. 1a**. Each Fe_3GeTe_2 unit has a thickness of five atomic layers. Clearly, there are two types of Fe atoms with different coordination environments, i.e., trivalent iron (Fe^{3+}) and divalent iron (Fe^{2+}). The middle of 2D Fe_3GeTe_2 is a $Fe^{2+}Ge$ layer, sandwiched by bottom and upper Fe^{3+} layers. The entire surface of each Fe^{3+} layer is then covered by the atomic layer of Te. The corresponding ratio of number of Fe^{3+} and Fe^{2+} is 2:1. The 2D Fe_3GeTe_2 is metallic,[13] as seen from both electronic band structure and total density of states (TDOS) in **Supplementary Fig. 1**. Non-magnetic (NM), FM, and antiferromagnetic (AFM) states are all considered to determine their ground spin configurations. The corresponding FM and various AFM configurations are shown in Supplementary **Fig. 2**. Our results indicate that 2D Fe_3GeTe_2 has FM ground state.

In addition to coordination environment, the Fe^{3+} and Fe^{2+} ions are more accurately distinguished in 2D Fe_3GeTe_2 by their different electronic behavior, which is confirmed by the charge density distributions in **Fig. 1b** and Bader charge on Fe atoms.[23] Around the Fe^{2+} ions, electrons are more localized than that around the Fe^{3+} sites. The electrons are localized between Fe^{2+} and Ge/Te ions, reflecting their covalent bonding characteristics. In comparison, more delocalized ionic bonding takes place between Fe^{3+} and Ge/Te ions. This difference between localized and delocalized electron distributions around the Fe^{3+} and Fe^{2+} ions is also supported by Bader charge analysis. There is a net charge transfer of about 0.4 electrons from Fe^{3+} ions to

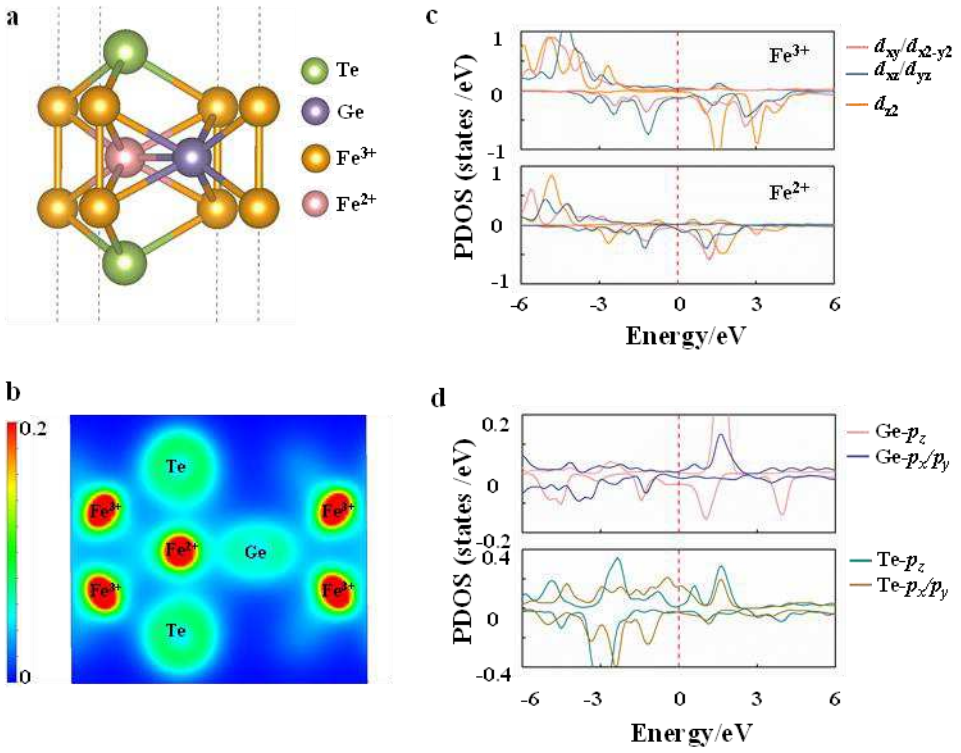

Fig. 1 Crystal and electronic structure of 2D Fe_3GeTe_2. a A schematic plot of the structure. The gold, pink, purple and green balls stand for Fe^{3+}, Fe^{2+}, Te and Ge ions. **b** Charge density for Fe_3GeTe_2 monolayer on the (110) face. **c** The orbital-projected density of states (PDOS) for Fe, Ge and Te atom, respectively. Among them, Fe atom could divide by trivalent iron Fe^{3+} and divalent iron Fe^{2+} The Fermi level (red dash line) is set to zero.

its surrounding Ge/Te ions. However, there is no evident charge transfer in the case of Fe^{2+} ions. Following this picture, we reveal the Fe^{2+} ion is localized relative to Fe^{3+} ion in 2D Fe_3GeTe_2, consistent with a previous report by Deiseroth *et al.*[24] The Co-existence of localized and itinerant magnetism have also been found in the iron-based superconductors and double perovskite materials, such as LaOFeAs, Sr_2FeMoO_6 and $La_{1-x}Sr_xMO_3$ (M=Mn and Co) [25, 26, 27, 28], which all are polyvalence materials.

The partial density of states (PDOS) can further clarify the origin of different electronic and magnetic features in Fe^{3+} and Fe^{2+} ions of 2D Fe_3GeTe_2, which shown in **Fig. 1**. Under a hexagonal crystal field, the five 3*d* orbitals of Fe atom split into a single state a_1 (d_{z2}), two twofold degenerate states e_1 (d_{x2-y2}/d_{xy}) and e_2 (d_{xz}/d_{yz}). From the PDOS of Fe atoms, one can

see that the d_{z2} orbital compared to the other 3*d* orbitals is obviously narrow and sharp that suggested a localized feature. However, the d_{x2-y2}, d_{xy}, d_{xz}, and d_{yz} orbitals in the minority-spin channels are obviously wide and them hybridized with Ge/Te-*p* states, indicating the delocalized feature. Similar to LaOFeAs, the localized *d*-electrons different from the itinerant electrons as coming from more isolated d_{z2} orbitals.[25] Moreover, 3*d* bands of the majority spin for both Fe^{3+} and Fe^{2+} ions are fully occupied, while those of the minority spin are partially occupied. These results indicate that both Fe^{3+} and Fe^{2+} ions are in their high-spin configurations. The main difference between Fe^{3+} and Fe^{2+} ions on PDOS is due to the d_{z2} and d_{xz}/d_{yz} states in the minority-spin channels. Specifically, the electron occupation number on minority d_{z2} orbital are 0.04 and 0.30 for Fe^{3+} and Fe^{2+} ions, respectively. That is to say, Fe^{2+} ion has ~0.3 more electron than Fe^{3+} ion to occupy the minority d_{z2} orbital. The occupied minority d_{z2} orbital results in Fe^{2+} ion is more localized than Fe^{3+} ion. In addition, compared to Fe^{2+} ion the energy level of minority d_{xz}/d_{yz} states of Fe^{3+} ion will shift to the lower energy region. The corresponding number of occupied minority d_{xz}/d_{yz} states increase from 0.35 to 0.54. Therefore, the resulting calculating net magnetic moment is 3.0 μ_B and 2.6 μ_B for Fe^{3+} and Fe^{2+} ions, respectively. The localized a_1 and delocalized e_1/e_2 states results in the unique magnetism in 2D Fe_3GeTe_2, which possessed the coexistence of local and itinerant magnetism, consistent with a previous report by Yang *et al*.[22] Obviously, the feature of localized magnetism play a crucial role in electronic and magnetism of metallic ferromagnetic Fe_3GeTe_2 system.

Magnetic coupling mechanism and Curie temperatures of 2D Fe_3GeTe_2

Because of the coexistence of localized and itinerant magnetism, the magnetic behavior of metallic ferromagnetic Fe_3GeTe_2 will deviate from itinerant Stoner model. Recently experiment indeed confirmed that metallic Fe_3GeTe_2 shown non-Stoner ferromagnetism. Yang *et al*. do not observe a considerable change in the electronic structure with temperature, which is not consistent with the expectation. Within the itinerant Stoner model, the ferromagnetic metal will exhibit a temperature-dependent exchange splitting that disappears above T_C.[22] Moreover, Tovar *et al.* used corrected Stoner parameter to describe the magnetic behaver in polyvalence Sr_2FeMoO_6, which also shown the coexistence of localized and itinerant magnetism. The corrections for Landau diamagnetism to Stoner parameter need to derived by experiment

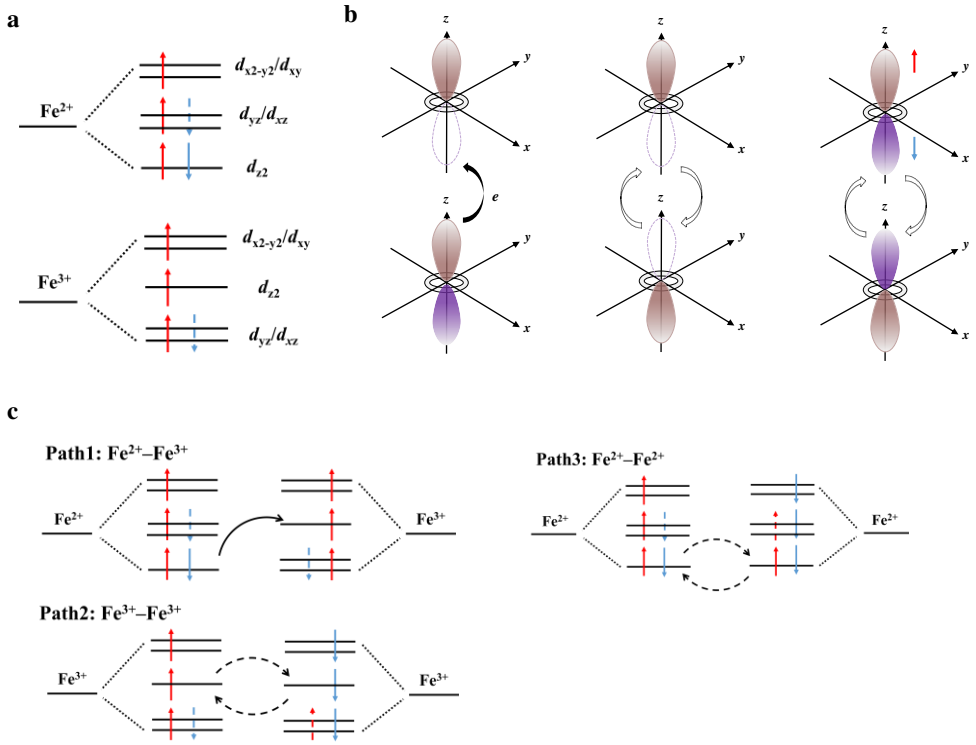

Fig. 2 The localized exchange in 2D Fe_3GeTe_2. a The schematic representation of splitting *d* orbital in Fe^{2+} and Fe^{3+} ions, respectively. **b** Three possible process of the exchange between localized d_{z2} orbital. **c** The corresponding three possible Fe–Fe exchange paths in Fe_3GeTe_2 crystal.

measured.[26] Therefore, we need a new model to describe the complicated ferromagnetism in Fe_3GeTe_2 systems.

In present paper, two main magnetic exchange mechanism have been introduced in 2D Fe_3GeTe_2. The itinerant magnetism between e_1 and e_2 electrons and localized magnetism in a_1 spins. Therefore, we propose a multipath magnetic interaction mechanism to understand the localized magnetic exchange for 2D Fe_3GeTe_2. According to the splitting of Fe^{2+} and Fe^{3+} orbitals in the crystal filed and multilayer structure of 2D Fe_3GeTe_2, three possible exchange paths are considered. **Fig. 2** shown the exchange paths between unoccupied d_{z2} orbital (Fe^{3+}–Fe^{3+}), occupied d_{z2} orbital (Fe^{2+}–Fe^{2+}) and unoccupied to occupied d_{z2} orbital (Fe^{2+}–Fe^{3+}), respectively. The hopping from the occupied Fe-d_{z2} orbitals to the unoccupied Fe-d_{z2} orbitals

induces extremely strong FM coupling (path $\boldsymbol{P_1}$), which occurs between the magnetic ions in different oxidation states, namely double exchange.[29] Double exchange play an essential role in polyvalence ferromagnetic materials like $La_{1-x}Sr_xMnO_3$ that also exhibited both localized and itinerant magnetism.[30] However, spin crossover between both unpaired Fe-d_{z2} orbitals (path $\boldsymbol{P_2}$) and paired Fe-d_{z2} orbitals (path $\boldsymbol{P_3}$) gives rise to an AFM interaction according to the Pauli exclusion principle. On the other hand, the non-spin-polarized PDOS (see Supplementary **Fig. 3**) shown that d_{xz}/d_{yz} and d_{x2-y2}/d_{xy} mainly contributed at the fermi level, and the lower kinetic energy makes them contributed to the itinerant ferromagnetism in 2D Fe_3GeTe_2. Therefore, the interaction between itinerant electrons in e_1 states endow the intralayer FM ($\boldsymbol{I_1}$), while the coupling between electrons in e_2 states favor in interlayer FM ($\boldsymbol{I_2}$). Among them, the intralayer FM only contributed by itinerant electrons ($\boldsymbol{I_1}$), but there is a competition between interlayer FM ($\boldsymbol{P_1}$ and $\boldsymbol{I_2}$) and AFM ($\boldsymbol{P_2}$ and $\boldsymbol{P_3}$) coupling. This explain why a debate regarding Fe atoms ferromagnetically or antiferromagnetically in Fe_3GeTe_2.[31] Moreover, Fu *et al*. also founded that the coexistence of localized and itinerant 3*d* electrons in $BiFeO_3/SrTiO_3$ superlattices and itinerant Fe-3*d* electrons tends to cause ferromagnetism.[32]

A local Heisenberg model can provides a good description of the ferromagnetic ordering in Fe_3GeTe_2 system.[14] In 2D Fe_3GeTe_2, there are three types of exchange interaction between Fe ions that correspond to the first, second and third nearest neighboring magnetic exchange constants J_1, J_2 and J_3, as shown in **Fig. 3a**. The value of J_1, J_2 and J_3 for 2D Fe_3GeTe_2 are extracted from the total energy difference between different spin orderings. As summarized in **Table 1**, the derived exchange interaction parameters are $J_1 = -0.44$ meV, $J_2 = 3.27$ meV, and $J_3 = 0.47$ meV. It is known that positive *J* value favors FM ordering, while negative *J* value favors AFM coupling. Therefore, the calculated J_1 of −0.44 meV yields weak AFM coupling, which occurs mainly through $\boldsymbol{P_2}$ path. The path $\boldsymbol{P_1}$ endows J_2 strong FM coupling with the value of 3.27 meV. Moreover, itinerant magnetism $\boldsymbol{I_1}$ and $\boldsymbol{I_2}$ making J_3 (0.47 meV) a long-range FM coupling. The coincidence between the magnetic interaction parameters and the effect of coexisting localized and itinerant magnetism, suggesting our proposed magnetic interaction mechanism is viable for understanding the magnetic ground state of 2D Fe_3GeTe_2. Its reliability is also verified by the other theoretical report. For example, first-principles calculations by Hu *et al.* have shown that the stability of ferromagnetism can be largely enhanced by tensile strain

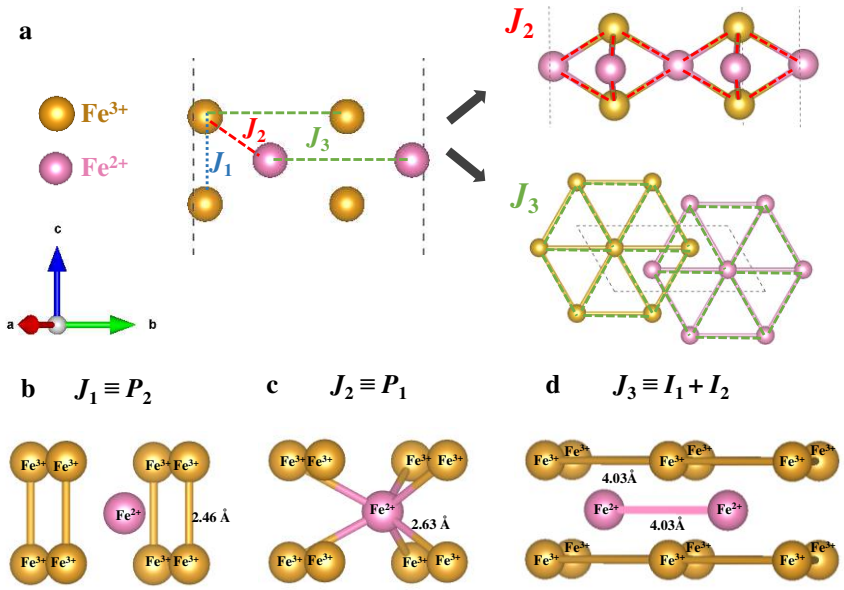

Fig. 3 Magnetic exchange parameter for 2D Fe_3GeTe_2. a The side view shows J_1 to J_3 for the Fe–Fe coupling in Fe_3GeTe_2 crystal. Fe–Fe exchange interaction paths for magnetic exchange constants in monolayer Fe_3GeTe_2. **b-d** The schematic diagrams of exchange parameters J_1, J_2 and J_3, respectively.

in Fe_3GeTe_2 monolayer.[33] Within our picture, tensile strain would shorten the Fe^{3+}–Fe^{2+} distance (***P*****1** path) but elongate the other interatomic distances, which in turn enhance the FM double exchange between Fe^{3+} and Fe^{2+} ions.

MAE as an important parameter of ferromagnets counteracts thermal fluctuations and preserves the long-range ferromagnetic ordering.[34] From non-collinear calculations with inclusion of the SOC effect, the MAE of 2D Fe_3GeTe_2 is determined as 0.94 meV/Fe, favoring perpendicular anisotropy, while the previously reported value was 0.67 meV/Fe.[14] For comparison, the MAE of 2.5 meV/Fe in bulk Fe_3GeTe_2 is slightly higher. The physical origin of positive MAE can be ascribed to the matrix element differences between the occupied and unoccupied spin-down *d* orbitals of Fe atom.[35] Roughly speaking, the coupling between occupied and unoccupied spin-down *d* orbitals of Fe atoms contribute to the major part of MAE. By decomposing the contribution from each pair of states, the MAE of 2D Fe_3GeTe_2 depend on the interaction between the a_1 and e_2 states. The positive contributions to MAE originate mainly

Table 1. The Fe^{2+}/Fe^{3+} ratio (x), effective thickness, formation energy (E_{form}), magnetic moment (M) per Fe atom, magnetic anisotropy energy (MAE) per unit cell, Curie temperature (T_C), and exchange parameters (J_1, J_2, J_3) of Fe_nGeTe_2 multilayer films.

	x	Thickness (Å)	E_{form} (eV/atom)	M (μ_B)	MAE (meV)	T_C (K)	Exchange parameter (meV)		
							J_1	J_2	J_3
Fe_3GeTe_2	0.5	8.61	–0.08	2.87	2.83	138	–0.44	3.27	0.47
Fe_4GeTe_2	1.0	9.10	–0.03	2.73	–5.01	68	7.40	10.50	0.10
Fe_5GeTe_2	0	10.95	–0.11	3.18	4.53	320	–0.20	4.70	–2.60
Fe_6GeTe_2	0.2	11.03	–0.05	2.94	6.31	450	6.60	–8.60	21.20
Fe_7GeTe_2	0.75	12.21	–0.01	2.91	3.91	570	–29.40	23.00	27.50

from unoccupied d_{z2} orbital and half-occupied d_{xz}/d_{yz} orbitals of Fe^{3+} ions, while the coupling of occupied d_{z2} and unoccupied d_{xz}/d_{yz} orbitals of Fe^{2+} ions exhibit the negative contribution to the MAE. Such mechanism also accounts for the variation of MAE for Fe_3GeTe_2 monolayer by decreasing Fe^{3+} content due to hole doping, as observed by Park *et al.*[36] Based on the obtained magnetic exchange constants and MAE, the Curie temperature of 2D Fe_3GeTe_2 is estimated using 2D Heisenberg model (see Supplementary **Fig. 4a**). The obtained T_C value of 138 K coincides well with previous experimental values of about 68–130 K for 2D Fe_3GeTe_2.[13, 14] The temperature-dependent magnetic moments (i.e., M-T curves) for each type of Fe ions (Fe^{3+} and Fe^{2+}) in Fe_3GeTe_2 compounds are also presented in Supplementary **Fig. 4b**. One can see that magnetizations of both Fe^{3+} and Fe^{2+} sublattices indeed behave like ferromagnets.

Fe_nGeTe_2 ultrathin films with tunable thickness

Additionally, most experimental phenomena about multilayer and bulk Fe_3GeTe_2 in previous reports could be explained by the coexistence states of localized and itinerant magnetism, signifying the validity of these magnetic interaction mechanisms. For example, the estimated T_C for bulk Fe_3GeTe_2 crystal is 280 K **(**see Supplementary **Fig. 5)**, which is comparable to the experimental value of 230 K.[24] Experimental study by Hwang *et al.* found

AFM coupling between pristine Fe_3GeTe_2 layer and oxidized Fe_3GeTe_2 layers. Their DFT calculations further revealed that such AFM coupling mainly originates from the oxygen atoms located at the interface of bilayer, while bilayer Fe_3GeTe_2 with oxygen atom adsorbed in the top or bottom sites still prefers FM state.[37] Within our localized Fe–Fe exchange model, the mediated oxygen atoms could provide an oxygen-mediated $\boldsymbol{P_2}$ path between two Fe_3GeTe_2 layers, which induces AFM coupling. Dai *et al.* reported a pressure-dependent phase diagram of Fe_3GeTe_2 thin flakes, and the magnetic transformation temperature from ferromagnetic to paramagnetic states is 203 K at 3.7 GPa and 163 K at 7.3 GPa, respectively. Moreover, the T_C shows an obviously descending trend from 4.0 GPa to 7.3 GPa because the reduction of local magnetic moment and increased of electronic itinerancy. [21] In the one hand, the increased electronic itinerancy could weaken the localized double exchange ($\boldsymbol{P_1}$ path). In the other hand, by analysis of their structural characteristics, we noticed that the Fe^{3+}–Te distance distinctly decreases before pressures of 7 GPa. The corresponding Fe^{3+}–Fe^{3+} exchange though the Te-mediated $\boldsymbol{P_2}$ path is stronger. The weaken FM coupling and enhanced AFM coupling, resulting in T_C is drastically reduced. Especially, the gate-tunable electrons sequentially fill the sub-bands origin from the Fe d_{z2}, d_{xz} and d_{yz} orbitals, induced room-temperature ferromagnetism in Fe_3GeTe_2.[14] The value of T_C mainly depended on the interaction between d_{z2}, d_{xz} and d_{yz} orbitals, consisting with our previously discuss. Moreover, the behavior from itinerant to localized magnetism enhanced the T_C, indicating the FM coupling in Fe_3GeTe_2 are mainly comes from the localized double exchange ($\boldsymbol{P_1}$ path).

The above discussions on the one hand demonstrate again the coexistence of itinerant and localized magnetism in Fe_3GeTe_2 system. On the other hand, the interlayer competition between localized exchange coupling (path $\boldsymbol{P_1}$, $\boldsymbol{P_2}$ and $\boldsymbol{P_3}$) and itinerant electrons ($\boldsymbol{I_1}$ and $\boldsymbol{I_2}$) is also crucial for the magnetic ground states, Curie temperature and MAE of 2D Fe_3GeTe_2. Moreover, the T_C was enhanced from 143 K to 226 K with the increase in Fe content from 2.75 to 3.10 in bulk $Fe_{3-x}GeTe_2$,[38] indicating the T_C is very sensitive to Fe content. These findings motivate us to explore new high-temperature Fe-Ge-Te systems with optimal Fe^{2+}/Fe^{3+} ratio and thickness, which the valence of Fe ions are related the direction of MAE and the competition of localized and itinerant magnetism in Fe_nGeTe_2 system. To satisfy these requirements, we have designed a series of Fe-rich Fe_nGeTe_2 ($4 \leq n \leq 7$) ultrathin films with various thickness (**Fig. 4**), which could

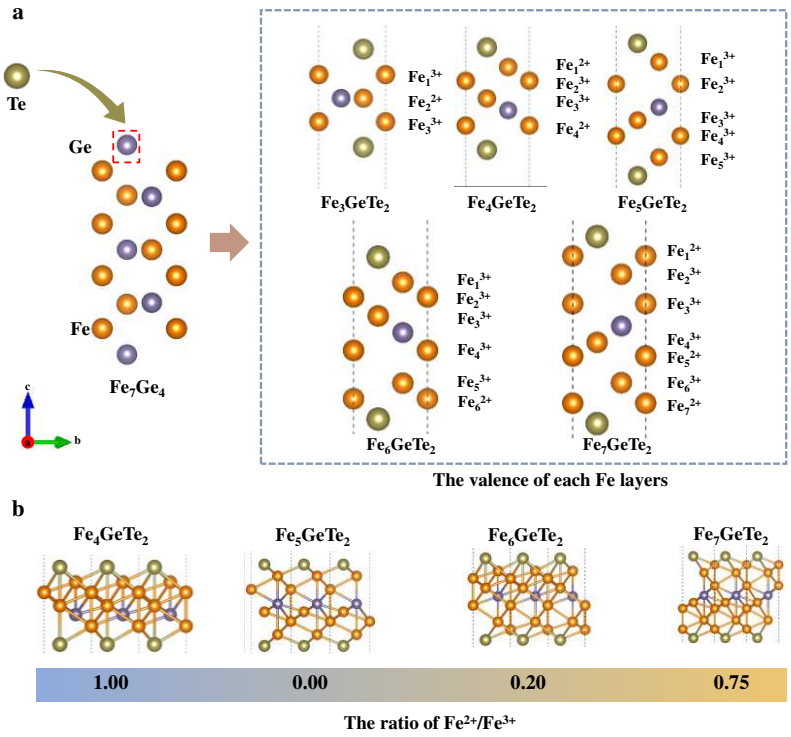

Fig. 4 Crystal strcture of Fe_nGeTe_2 ($4 \leq n \leq 7$). a Schematic illustration of Te-substituted Fe_7Ge_4 crystal and constituted five structures in the series of Fe_nGeTe_2. **b** The stacked plane views of Fe_nGeTe_2 multilayer films with difference Fe^{2+}/Fe^{3+} ratio along [001] direction.

exhibit abundant magnetism by more complicated competition between itinerant and localized magnetism in multilayer structure. Similar to the 2D Fe_3GeTe_2, Fe_nGeTe_2 ultrathin films also belong to *P*-3*m*1 space group. The effective thicknesses (**Table 1**) of Fe_4GeTe_2, Fe_5GeTe_2, Fe_6GeTe_2, Fe_7GeTe_2 ultrathin films are 5.63 Å, 6.79 Å, 7.56 Å, and 8.73 Å, respectively, which are moderately larger than that of Fe_3GeTe_2 (5.14 Å). The atomic arrangement of Fe_nGeTe_2 ultrathin films can be regarded as six, seven, eight, and nine atomic layered thickness (001) surface of Te-substituted Fe_7Ge_4 crystal.[39] Fortunately, the atomic arrangement of five atomic layered thickness Te-substituted Fe_7Ge_4 crystal is the same as the experimentally reported Fe_3GeTe_2 phase. To further check the experimentally feasibility of Fe_nGeTe_2, we calculated their formation energies, which is defined as

$$E_f = [E(Fe_nGeTe_2) - E(Fe_2Ge) - E(Te_2) - (n-3)E(Fe)]/(n+3) \quad (6)$$

where $E(Fe_nGeTe_2)$ represents the total energy of 2D Fe_nGeTe_2 compound, and $E(Fe_2Ge)$, $E(Te_2)$ and $E(Fe)$ are the total energy for Fe_2Ge, Te and Fe in their most stable bulk phase, respectively.[40] The formation energies of four Fe_nGeTe_2 ultrathin films from our theoretical design are –0.03 eV/atom (n = 4), –0.11 eV/atom (n = 5), –0.05 eV/atom (n = 6), and –0.01 eV/atom (n = 7), respectively, which are comparable to the formation energy of –0.08 eV/atom for Fe_3GeTe_2. All these negative values indicate that their formation processes are exothermic. More importantly, we find that the total energy of our proposed Fe_5GeTe_2 ultrathin film is 0.24 eV per atom lower than that of the experimentally reported layered phase with same stoichiometry.[16] The satisfactory stability of these Fe_nGeTe_2 ultrathin film implies that they are feasible from the theoretical point of view. It is noteworthy that ultrathin films of Cr_2S_3, CrSe and FeTe in FM state have been synthesized by CVD and MBE methods in previous experiments.[11, 12, 41]

Magnetic behavior of Fe_nGeTe_2 ultrathin films

We further discuss the electronic and magnetic properties of the proposed Fe_nGeTe_2 ultrathin films. Similar to 2D Fe_3GeTe_2, all Fe_nGeTe_2 systems are metallic, as seen from the electronic band structures in Supplementary **Fig. 6**. The orbital project densities of states in Supplementary **Fig. 7** demonstrate that the metallicity still originate from *d* orbitals of Fe atoms. The coexistence of itinerant and localized *d* electrons in Fe_nGeTe_2 ($3\leq n\leq 7$) could revealed by the Bader charge (see Supplementary **Table 1**) and PDOS. The distribution of Fe^{2+} and Fe^{3+} ions vary with the thickness and compositions of 2D Fe_nGeTe_2 ultrathin films. With increasing Fe content, the Fe^{2+}/Fe^{3+} (x) ratio is 0.5, 1.0, 0, 0.2, and 0.75 for n = 3, 4, 5, 6, and 7, respectively, which represented a magnetic behave from itinerant to localized. In order to investigate the ground states of Fe_nGeTe_2 ultrathin films, we considered FM and various AFM configurations (see Supplementary **Fig. 8**). Due to the multilayer structures, the considered AFM configurations are increased with the Fe content. From our DFT calculations, FM ordering in all Fe_nGeTe_2 systems is more favorable than the AFM or NM counterparts. The magnetic moments as a function of x is plotted in **Fig. 5a**. With increasing Fe^{2+}/Fe^{3+} ratio, the average magnetic moments per Fe atom slightly declines from 3.18 μ_B for x = 0 to 2.87 μ_B for x = 1. This observation can be easily understood that Fe^{3+} ions contribute larger magnetic moment

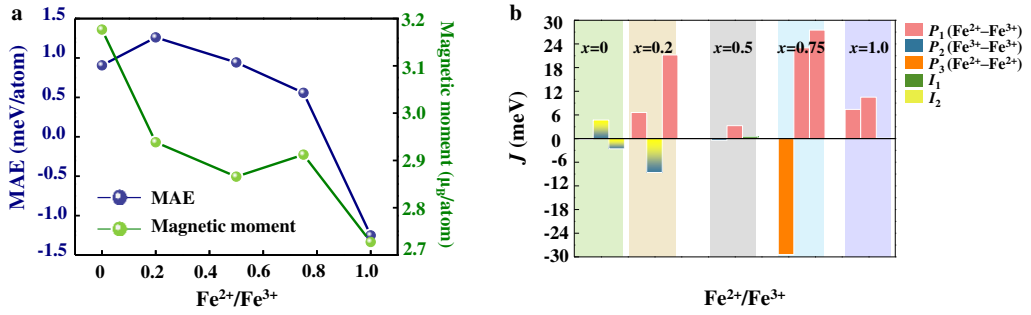

Fig. 5 Magnetic properties of multilayer Fe_nGeTe_2. **a** The Calculated MAE and magnetic moment per atom at various Fe^{2+}/Fe^{3+} ratio (x). The detailed data are listed in Table 1. **b** The exchange parameters for first, second and third nearest neighbor (see Supplementary **Fig. 9**). The green, gold, gray, blue and purple regions represent $x = 0$, 0.2, 0.5, 0.75 and 1.0, respectively.

than Fe^{2+} ions. In other words, the itinerant behavior of *d* orbitals is weakened as the Fe^{2+}/Fe^{3+} ratio increases.

Because the T_C in Fe_nGeTe_2 systems are mainly come from localized double exchange, we considered the exchange parameters J of Fe_nGeTe_2 ultrathin film that are presented in **Table 1** and Supplementary **Fig. 9**. Meanwhile, the long-range magnetic coupling with $J = 5$ instead of $J = 3$ exchange parameters has been considered in Fe_nGeTe_2 (n= 5 to 7) with the Fe content increased. (see Supplementary **Table 2**). Before the Fe^{2+}/Fe^{3+} ratio up to 0.5, their magnitude and sign is insensitive to the distance of magnetic ion pairs and obviously existed a competition between localized and itinerant magnetism. With the Fe^{2+}/Fe^{3+} ratio continually increased, the localized magnetic exchange are dominant and their magnitude decreased with the distance of Fe ions. Meanwhile, the variations of J_1, J_2, and J_3 can be also interpreted by magnetic interaction mechanism, which has been established in the 2D Fe_3GeTe_2 earlier.

To further clarify the magnetic ground states of 2D Fe_nGeTe_2 ultrathin films, the relationship between exchange path dependent parameters J_1, J_2, and J_3 with Fe^{2+}/Fe^{3+} ratio x is displayed in **Fig. 5b**, from which we can raise several arguments. First, due to the exchange through d_{z2} and d_{xz}/d_{yz} orbital are dominant in multilayer structures, the strength of interlayer localized d_{z2} orbital interactions (***P*₁**, ***P*₂** and ***P*₃** paths) and itinerant electrons coupling of d_{xz}/d_{yz} orbital (***I*₂**) prevail over the intralayer interactions (***I*₁** path) in Fe_nGeTe_2 systems. Secondly, for

all the Fe_nGeTe_2 systems considered here, the dominant J parameter for FM coupling mainly comes from double exchange of localized d_{z2} orbital (***P*₁** path) and itinerant electrons of d_{xz}/d_{yz} orbitals coupling (***I*₂**). But the major J parameter for AFM ordering is mainly from the couplings between the localized d_{z2} orbitals in Fe^{3+}–Fe^{3+} and Fe^{2+}–Fe^{2+} exchange (***P*₂** and ***P*₃** paths). Therefore, the competition between interlayer AFM and FM coupling derived from the struggle between the itinerant and localized magnetism in Fe^{2+}–Fe^{2+} or Fe^{3+}–Fe^{3+} coupling. In Fe_5GeTe_2 ultrathin film, when the distance of interlayer Fe layers is shortly the localized magnetic exchange through ***P*₂** path could compete with itinerant e_2 electrons. However, the itinerant e_2 electrons become dominant with the Fe–Fe distance increased such as the value of J_4 is 5.9 meV. Subsequently, the itinerant magnetism weakens with the Fe–Fe distance continued increased, which the value of J_5 is 0.1 meV. Two competing ferromagnetism of localized and itinerant are responsible for these complicated behavior of the magnetic exchange parameters. As Fe^{2+}/Fe^{3+} ratio increases, more localized ***P*₁**/***P*₃** path (FM/AFM) and less ***I*₂** (FM) could be introduced; thus there is no simple trend for the variation of J parameters.

The MAE values for all the Fe_nGeTe_2 ultrathin films with different Fe^{2+}/Fe^{3+} ratios are also shown in **Fig. 5a**. One can see that MAE first increases from 0.91 meV/Fe atom for $x = 0$ (Fe_5GeTe_2) to 1.05 meV/Fe atom for $x = 0.2$ (Fe_6GeTe_2). Then, it almost monotonically decreases with increasing Fe^{2+}/Fe^{3+} ratio in the mixed-valence Fe_nGeTe_2 compounds. As the x further increases to 1, the easy axis would flip from perpendicular into in-plane orientation. The amplitude and direction of magnetic anisotropy are affected by two competing factors simultaneously. One is the Fe^{2+}/Fe^{3+} ratio. As we have discussed in 2D Fe_3GeTe_2, Fe^{3+} and Fe^{2+} ions contribute to positive and negative MAE, respectively. Another important factor is the interaction between d_{z2} and d_{xz}/d_{yz} orbitals, since the electronic band structures reveal that the spin-minority components of these orbitals are affected by spin-orbit coupling associated with the inserted Fe layers. To further unveil the origin of MAE enhancement from Fe_5GeTe_2 to Fe_6GeTe_2, we decomposed the MAE to the coupling of d_{z2} and d_{xz}/d_{yz} pairs by Eq.(2) (see Supplementary **Fig. 10**). When Fe^{2+}/Fe^{3+} ratio is 0 (Fe_5GeTe_2), there only exist positive contributions of occupied d_{xz}/d_{yz} and unoccupied d_{z2} pair with the difference in orbital energy levels of about 4.08 eV, leading to an out-of-plane MAE of 0.91 meV/Fe atom. With Fe^{2+}/Fe^{3+} ratio increases from 0 (Fe_5GeTe_2) to 0.2 (Fe_6GeTe_2), the energy level differences between

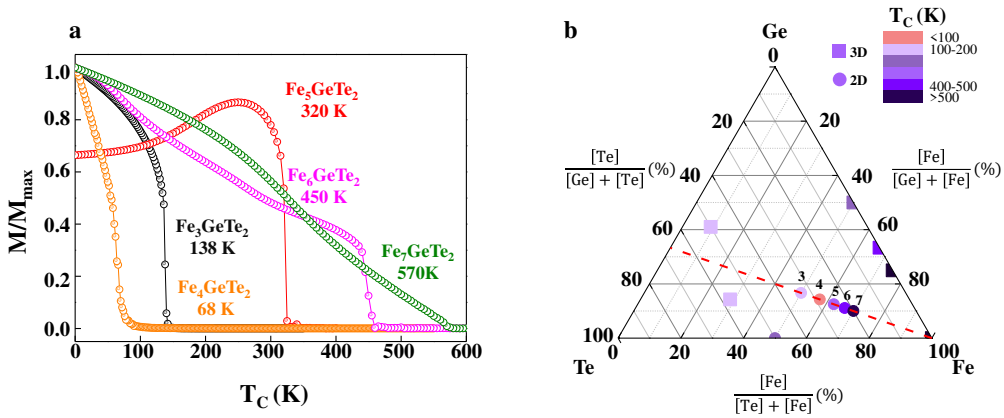

Fig. 6 Thickness-dependent magnetic properties of multilayer Fe_nGeTe_2 and comparison with other Fe-rich ferromagnets. a Calculated normalized magnetization of Fe atoms in Fe_nGeTe_2 as a function of temperature from MC simulation. **b** Ternary phase diagram of various Fe-rich compositions, together with the stoichiometric line of Fe:Ge:Te = n:1:2 ($3 \leq n \leq 7$). The color indicates the value of T_C. The squares and circles represent 3D and 2D strctures, respectively.

occupied d_{xz}/d_{yz} and unoccupied d_{z2} pair and unoccupied d_{xz}/d_{yz} and occupied d_{z2} pair are 3.79 and 4.65 eV, respectively. Therefore, for the occupied d_{xz}/d_{yz} and unoccupied d_{z2} pair, the positive contributions to MAE prevail the negative contributions.

Using these exchange parameters and MAE strengths, we have evaluated the total M-T curves of Fe_nGeTe_2 systems, as shown in **Fig. 6a**. We have also simulated the M-T curves for every Fe sublattices (see Supplementary **Fig. 11)**. For various stoichiometries, three kinds of M-T curves are observed. Similar to Fe_3GeTe_2, Fe_4GeTe_2 is also a true ferromagnet. The magnetic spin moments of all Fe atoms align in the same direction, and they decrease with increasing temperature, yielding a T_C value of 68 K. For Fe_5GeTe_2, the magnetic moment keeps increasing with temperature, and full compensation is not observed in the entire temperature range. The maximum in spontaneous magnetization appears between the 0 K and T_C (320 K). For each Fe sublattice, the Fe_1 and Fe_5 layers are thermally disturbed more easily and their magnetic moments almost decrease linearly with increasing temperature, while the other three layers (Fe_2, Fe_3, and Fe_4) drastically decrease around 320 K. As a result, Fe_5GeTe_2 behaves as

a Néel's P-type ferrimagnet. The ferrimagnetic to paramagnetic transition occurs at a critical temperature of T_C = 320 K. According to Néel's classification of ferrimagnets,[42] 2D Fe_6GeTe_2 and Fe_7GeTe_2 sheets are the Néel's R-types. Their M-T curves exhibit monotonic reduction with increasing temperature. For the Fe sublattices of Fe_6GeTe_2, the spin moments of Fe_1, Fe_3, Fe_4, Fe_5, and Fe_6 layers and Fe_2 layers show opposite directions, while all the moments decrease with temperature. For the M-T curves of 2D Fe_7GeTe_2, the spin directions of Fe_2, Fe_4 and Fe_5 layers and Fe_1, Fe_3 Fe_6 and Fe_7 layers are opposite. The ferrimagnetic to paramagnetic transition occurs at T_C of 570 K. The present Néel's R- and P-types of magnetization profiles have also been reported in mixed-valence complex alloys ($Mn_{1.5}FeV_{0.5}Al$ [43] and $Mn_2V_{0.5}C_{0.5}Z$ [44]), complex oxides ($NiCo_2O_4$[45]), layered materials ($AFe^{II}Fe^{III}(C_2O_4)_3$ [46]) and core-shell nanoparticles [47]. The competition of interlayer AFM and FM coupling resulting in the transition from FM to FiM states in Fe_nGeTe_2, deriving from the coexistence of different electronic states.

The simulated T_C are 138 K for Fe_3GeTe_2, 68 K for Fe_4GeTe_2, 320 K for Fe_5GeTe_2, 450 K for Fe_6GeTe_2, and 570 K for Fe_7GeTe_2, respectively. For the truly ferromagnetic systems, T_C drops from 138 K for Fe_3GeTe_2 to 68 K for Fe_4GeTe_2 because of the flipping of out-of-plane MAE brought by the increased ratio of Fe^{2+} ions. Further increasing Fe content leads to a transition of magnetic ordering from ferromagnetic to ferrimagnetic at Fe_5GeTe_2. For $n \geq 5$, T_C of the ferrimagnetic Fe_nGeTe_2 film increases with n, mainly due to higher MAE and stronger double exchange. The similar trend have also been observed in ferromagnetic $Fe_{3-x}Cr_xGe$ and $Fe_{3-x}V_xGe$ alloys.[48, 49] By extrapolating to even thicker films, Fe_nGeTe_2 with n = 9 and an effective thickness of 14 Å yields a T_C = 1006 K, which is comparable to T_C = 1043 K for pure Fe solid of bcc phase[15] (see Supplementary **Fig. 12)**.

Ternary phase diagram of T_C for Fe based compounds

In order to provide a more general aspect to the composition and dimensional effects on the magnetic behavior of Fe-Ge-Te systems, we plot a ternary phase diagram of T_C for various reported Fe based compounds (**Fig. 6b**). In the three-dimensional (3D) compounds, the T_C of Fe-rich composition monotonically increases from 279 K for FeGe [50] to 485 K for Fe_2Ge [51], and then to 1043 K for pure Fe,[15] showing a prominent composition effect. In the 2D Fe-Ge-Te films, T_C is determined by the combined composition and dimensional effects. Generally

speaking, incorporation of Fe atoms in the system would increase T_C. For example, Fe doping generates the long-range spin ordering in GeTe films and the T_C of $Fe_{0.18}Ge_{0.82}Te$ films is 100 K.[52] The T_C of our Fe_3GeTe_2 (138 K) with effective thickness of 0.86 nm is lower than the FeTe ultrathin film with 2.80 nm (T_C = 220 K)[12], even with the same Fe content. Moreover, the T_C of Fe_6GeTe_2 (450 K) is slightly lower to the bulk Fe_2Ge phase (T_C = 485 K). Both of them have Fe content of 0.67. However, the role of non-metal element (Ge and Te) inclusion in the ultrathin Fe-Ge-Te films is very complicated. They can not only tune the chemical valence state and the electronic behavior of the variable element Fe but also provide crystal field to control MAE, which will change the magnetic behave and T_C.

Discussion

We design a family of 2D Fe_nGeTe_2 ultrathin films with different Fe contents and thickness, which are experimentally more feasible than the reported 2D layered phase. By first-principle calculations, we systemically study their electronic and magnetic properties, and reveal some important findings to obtain low dimensional magnetic materials with high working temperature. All the 2D Fe_nGeTe_2 ultrathin films considered here are robust ferromagnetic/ferrimagnetic with magnetic transition temperature of 68-570 K, which can be ascribed to the coexistence of itinerant and localized electronic state. The localized magnetism comes from the electrons in d_{z2} orbital, while the itinerant magnetism derive from electrons in $d_{xz}/d_{yz}/d_{xy}/d_{x2-y2}$ orbitals. The coexistence of itinerant and localized electronic states also shows a good correlation with many critical magnetic parameters, such as magnetic moment, exchange parameters, MAE and T_C, which have been carefully discussed in this paper. Based on these results, we propose a localized Fe–Fe exchange Heisenberg model, which can be well described the exchange between the d_{z2} orbitals in FGT systems. It may also suitable to the variable valence element-based magnetic compounds. Meanwhile, the itinerant magnetism introduced to our mechanism to explain the competitive intra- and interlayer ferromagnetism. Moreover, the established thickness-dependent magnetic order suggests the possibility of tuning the interlayer exchange energy of Fe-Ge-Te system by changing the composition. Our studies are very helpful to understand the modulating effect of thickness on 2D Fe_nGeTe_2 ultrathin films

with variable valence elements and indicate that 2D magnetic Fe_nGeTe_2 ultrathin films can be a very promising candidate for future room temperature spintronic applications.

Methods

First-principle calculations. Our first-principles calculations were based on density functional theory (DFT) within the generalized gradient approximation (GGA),[53] as implemented in the VASP code.[54] The projected augmented wave (PAW) potentials was used to describe the ion-electron interaction.[55] The energy cutoff of plane wave basis was set as 500 eV. A vacuum space of 20 Å thickness was added to avoid the interaction between adjacent layers. During geometry optimization, a Monkhorst-Pack **k**-point mesh of 0.02 $Å^{-1}$ were chosen for sampling the 2D Brillouin zones. To remove the self-interaction errors, the effective Hubbard U parameter (U = 4.3 eV) was included within the PBE+U framework, which is consistent with previous studies.[56, 57] Correction of van der Waals interactions using the DFT-D3 scheme,[58] was included in the bulk Fe_3GeTe_2 calculations.

To describe the magnetic properties of Fe_nGeTe_2 crystals, the magnetic anisotropy energy (MAE) is defined as

$$\mathrm{MAE} = E_{\mathrm{tot}}[100] - E_{\mathrm{tot}}[001] \quad (1)$$

where $E_{\mathrm{tot}}[100]$ and $E_{\mathrm{tot}}[001]$ refer to the total energies of states whose magnetization direction is parallel and perpendicular to the basal plane, respectively.[59]

In the present system, the minority spin states dominate the magnetic anisotropy, such that the MAE can be expressed as[60]

$$\mathrm{MAE} \approx \Delta \mathrm{E}^{\mathrm{dd}} = (\xi)^2 \sum_{\mathrm{o}^-\mathrm{u}^-} \frac{|\langle o^-|L_z|u^-\rangle|^2 - |\langle o^-|L_x|u^-\rangle|^2}{\varepsilon_{\mathrm{u}^-} - \varepsilon_{\mathrm{o}^-}} \quad (2)$$

Here, L_x and L_z are the x and z components of angular momentum operator, and o and u denote the spin-down orbital in the occupied and unoccupied states, respectively. From Eq.(2), we know that $\Delta \mathrm{E}^{\mathrm{dd}}$ is not only determined by the orbital character of the occupied states but also depends on the coupling with the empty states and splitting between them through the energy denominator.

Moreover, Monte Carlo (MC) simulations have been carried out to determine the magnetic transition temperatures. The Hamiltonian of the system is expressed as following form

$$H = -\sum_{(ij)} J_{ij} \vec{S}_i \cdot \vec{S}_j - K \sum_i \left(\vec{S}_i \cdot \vec{e}_i \right)^2 \tag{3}$$

where $\vec{S}_i$ is the unit vector of the magnetic moment at the site i; J_{ij} represents the exchange-coupling constant between magnetic Fe atoms; K is the anisotropy constant and $\vec{e}_i$ is the unit vector along the easy direction of the magnetic anisotropy. The parameters used in the MC simulations were obtained from first-principles calculations. To determine the Curie temperature, the magnetization M per atom and the specific heat C_m are calculated by

$$M = \left\langle \left[\left(\sum_i S_i^x \right)^2 + \left(\sum_i S_i^y \right)^2 + \left(\sum_i S_i^z \right)^2 \right]^{1/2} \right\rangle \Big/ N \tag{4}$$

and

$$C_m = \left(\left\langle E^2 \right\rangle - \left\langle E \right\rangle^2 \right) \Big/ N k_B T^2 \tag{5}$$

respectively. Here N is the total number of magnetic Fe atoms, and k_B denotes the Boltzmann constant. The simulation supercells were constructed by 50×50 expansion of the unit cell. For each temperature, the first 10^5 MC steps were discarded for thermal equilibration; the successive 10^5 MC steps were then used to collect data and determine the thermodynamic averages of given physical quantities. Indeed, all thermodynamic properties were averaged over five different seed numbers.

Data availability

The data that support the findings of this study are available from the corresponding author on reasonable request.

References

1. Huang, B. et al. Layer-dependent ferromagnetism in a van der Waals crystal down to the monolayer limit. *Nature* **546**, 270-273 (2017).
2. McGuire, M. Crystal and Magnetic Structures in Layered, Transition Metal Dihalides and Trihalides. *Crystals* **7**, 121 (2017).
3. Li, Z., Zhou, B. & Luan, C. Strain-tunable magnetic anisotropy in two-dimensional Dirac half-metals: nickel trihalides. *RSC Adv.* **9**, 35614-35623 (2019).
4. Gong, C. et al. Discovery of intrinsic ferromagnetism in two-dimensional van der Waals crystals. *Nature* **546**, 265-269 (2017).
5. Vatansever, E. et al. Strain effects on electronic and magnetic properties of the monolayer α-$RuCl_3$: A first-principles and Monte Carlo study. *J. Appl. Phys.* **125**, 083903 (2019).
6. Ersan, F. et al. Exploring the electronic and magnetic properties of new metal halides from bulk

to two-dimensional monolayer: RuX_3 (X = Br, I). *J. Magn. Magn. Mater.* **476**, 111-119 (2019).
7. Goodenough, J. B. Theory of the Role of Covalence in the Perovskite-Type Manganites [La, *M*(II)]MnO_3. *Phys. Rev.* **100**, 564-573 (1955).
8. Kanamori, J. Crystal Distortion in Magnetic Compounds. *J. Appl. Phys.* **31**, S14-S23 (1960).
9. Anderson, P. W. New Approach to the Theory of Superexchange Interactions. *Phys. Rev.* **115**, 2-13 (1959).
10. Bhatti, S., Sbiaa, R., Hirohata, A., Ohno, H., Fukami, S. & Piramanayagam, S. N. Spintronics based random access memory: a review. *Mater. Today* **20**, 530-548 (2017).
11. Zhang, Y. et al. Ultrathin Magnetic 2D Single-Crystal CrSe. *Adv. Mater.* **31**, 1900056 (2019).
12. Kang, L. et al. Phase-controllable growth of ultrathin 2D magnetic FeTe crystals. *Nat. Commun.* **11**, 3729 (2020).
13. Fei, Z. et al. Two-dimensional itinerant ferromagnetism in atomically thin Fe_3GeTe_2. *Nat. Mater.* **17**, 778-782 (2018).
14. Deng, Y. et al. Gate-tunable room-temperature ferromagnetism in two-dimensional Fe_3GeTe_2. *Nature* **563**, 94-99 (2018).
15. Seo, J. et al. Nearly room temperature ferromagnetism in a magnetic metal-rich van der Waals metal. *Sci. Adv.* **6**, eaay8912 (2020).
16. May, A. F. et al. Ferromagnetism Near Room Temperature in the Cleavable van der Waals Crystal Fe_5GeTe_2. *ACS Nano* **13**, 4436-4442 (2019).
17. Yuan, Q.-Q. et al. Ferromagnetic MnSn Monolayer Epitaxially Grown on Silicon Substrate. *Chinese Phys. Lett.* **37**, 077502 (2020).
18. Abdullahi, Y. Z., Vatansever, Z. D., Ersan, F., Akinci, U., Akturk, O. U. & Akturk, E. Ferromagnetic TM_2BC (TM = Cr, Mn) monolayers for spintronic devices with high Curie temperature. *Phys. Chem. Chem. Phys.* **23**, 6107-6115 (2021).
19. Gökoğlu, G. & Aktürk, E. Half metallicity and pressure-induced electronic structure of monolayer FeX_2 (X = S, Se). *Mater. Res. Express* **4**, 116305 (2017).
20. Stoner, E. C. Collective electron ferronmagnetism. *Proceedings of the Royal Society of London. Series A. Mathematical and Physical Sciences* **165**, 372-414 (1938).
21. Wang, H. et al. Pressure-Dependent Intermediate Magnetic Phase in Thin Fe_3GeTe_2 Flakes. *J. Phys. Chem. Lett.* **11**, 7313-7319 (2020).
22. Xu, X. et al. Signature for non-Stoner ferromagnetism in the van der Waals ferromagnet Fe_3GeTe_2. *Phys. Rev. B* **101**, 201104 (2020).
23. Henkelman, G., Arnaldsson, A. & Jónsson, H. A fast and robust algorithm for Bader decomposition of charge density. *Comp. Mater. Sci.* **36**, 354-360 (2006).
24. Deiseroth, H.-J., Aleksandrov, K., Reiner, C., Kienle, L. & Kremer, R. K. Fe_3GeTe_2 and Ni_3GeTe_2 – Two New Layered Transition-Metal Compounds: Crystal Structures, HRTEM Investigations, and Magnetic and Electrical Properties. *Eur. J. Inorg. Chem.* **2006**, 1561-1567 (2006).
25. Kou, S.-P., Li, T. & Weng, Z.-Y. Coexistence of itinerant electrons and local moments in iron-based superconductors. *Europhys. Lett.* **88**, 17010 (2009).
26. Tovar, M. et al. Evidence of strong antiferromagnetic coupling between localized and itinerant electrons in ferromagnetic Sr_2FeMoO_6. *Phys. Rev. B* **66**, 024409 (2002).
27. Edwards, D. M. Ferromagnetism and electron-phonon coupling in the manganites. *Adv. Phys.* **51**, 1259-1318 (2002).

28. Bhide, V. G., Rajoria, D. S., Rao, C. N. R., Rao, G. R. & Jadhao, V. G. Itinerant-electron ferromagnetism in $La_{1-x}Sr_xCoO_3$: A Mössbauer study. *Phys. Rev. B* **12**, 2832-2843 (1975).
29. Stöhr, J. & Siegmann, H. C. *Magnetism* (Springer-Verlag, Berlin, Germany, 2006).
30. Moritomo, Y., Asamitsu, A. & Tokura, Y. Pressure effect on the double-exchange ferromagnet $La_{1-x}Sr_xMnO_3$ (0.15<=x<=0.5). *Phys. Rev. B* **51**, 16491-16494 (1995).
31. Yi, J. et al. Competing antiferromagnetism in a quasi-2D itinerant ferromagnet: Fe_3GeTe_2. *2D Materials* **4**, 011005 (2016).
32. Fu, Z., Chen, H., Liu, Y., Liu, M. & Liu, W.-M. Interface-induced ferroelectric domains and charged domain walls in $BiFeO_3/SrTiO_3$ superlattices. *Phys. Rev. B* **103**, 195301 (2021).
33. Hu, X., Zhao, Y., Shen, X., Krasheninnikov, A. V., Chen, Z. & Sun, L. Enhanced Ferromagnetism and Tunable Magnetism in Fe_3GeTe_2 Monolayer by Strain Engineering. *ACS Appl. Mater. Inter.* **12**, 26367-26373 (2020).
34. Shabbir, B. et al. Long range intrinsic ferromagnetism in two dimensional materials and dissipationless future technologies. *Appl. Phys. Rev.* **5**, 041105 (2018).
35. Wang, P., Jiang, X., Hu, J. & Zhao, J. Chemically Engineering Magnetic Anisotropy of 2D Metalloporphyrin. *Adv. Sci.* **4**, 1700019 (2017).
36. Park, S. Y. et al. Controlling the Magnetic Anisotropy of the van der Waals Ferromagnet Fe_3GeTe_2 through Hole Doping. *Nano Lett.* **20**, 95-100 (2020).
37. Kim, D. et al. Antiferromagnetic coupling of van der Waals ferromagnetic Fe_3GeTe_2. *Nanotechnology* **30**, 245701 (2019).
38. May, A. F., Calder, S., Cantoni, C., Cao, H. & McGuire, M. A. Magnetic structure and phase stability of the van der Waals bonded ferromagnet $Fe_{3-x}GeTe_2$. *Phys. Rev. B* **93**, 014411 (2016).
39. Villars, P., Calvert, L. D. & Pearson, W. B. Handbook of Crystallographic Data for Intermetallic Phases. *Acta Crystallogr. A* **40**, C444 (1984).
40. Behler, J. Atom-centered symmetry functions for constructing high-dimensional neural network potentials. *J. Chem. Phys.* **134**, 074106 (2011).
41. Chu, J. et al. Sub-millimeter-Scale Growth of One-Unit-Cell-Thick Ferrimagnetic Cr_2S_3 Nanosheets. *Nano Lett.* **19**, 2154-2161 (2019).
42. Néel, M. L. Propriétés magnétiques des ferrites ; ferrimagnétisme et antiferromagnétisme. *Ann. Phys.* **12**, 137-198 (1948).
43. Stinshoff, R. et al. Completely compensated ferrimagnetism and sublattice spin crossing in the half-metallic Heusler compound $Mn_{1.5}FeV_{0.5}Al$. *Phys. Rev. B* **95**, 060410 (2017).
44. Midhunlal, P. V., Arout Chelvane, J., Prabhu, D., Gopalan, R. & Harish Kumar, N. $Mn_2V_{0.5}Co_{0.5}Z$ (Z = Ga, Al) Heusler alloys: High T_C compensated P-type ferrimagnetism in arc melted bulk and N-type ferrimagnetism in melt-spun ribbons. *J. Magn. Magn. Mater.* **489**, 165298 (2019).
45. Bitla, Y. et al. Origin of metallic behavior in $NiCo_2O_4$ ferrimagnet. *Sci. Rep-UK* **5**, 15201 (2015).
46. Nuttall, C. J. & Day, P. Magnetization of the Layer Compounds $AFe^{II}Fe^{III}(C_2O_4)_3$ (A = Organic Cation), in Low and High Magnetic Fields: Manifestation of Néel N and Q Type Ferrimagnetism in a Molecular Lattice. *Chem. Mater.* **10**, 3050-3057 (1998).
47. Vatansever, E. & Polat, H. Monte Carlo investigation of a spherical ferrimagnetic core–shell nanoparticle under a time dependent magnetic field. *J. Magn. Magn. Mater.* **343**, 221-227 (2013).
48. Mahat, R. et al. Tuneable structure and magnetic properties in $Fe_{3-x}V_x$ Ge alloys. *J. Alloys Compd.* **830**, 154403 (2020).

49. Mahat, R. et al. Influence of Cr-substitution on the structural, magnetic, electron transport, and mechanical properties of $Fe_{3-x}Cr_xGe$ Heusler alloys. *J. Magn. Magn. Mater.* **521**, 167398 (2021).
50. Xu, L. et al. Magnetic entropy change and accurate determination of Curie temperature in single-crystalline helimagnet FeGe. *Europhys. Lett.* **117**, 47004 (2017).
51. Yasukōchi, K., Kanematsu, K. & Ohoyama, T. Magnetic Properties of Intermetallic Compounds in Iron-Germanium System : $Fe_{1.67}Ge$ and $FeGe_2$. *J. Phys. Soc. Jpn.* **16**, 429-433 (1961).
52. Fukuma, Y., Asada, H., Miyashita, J., Nishimura, N. & Koyanagi, T. Magnetic properties of IV–VI compound GeTe based diluted magnetic semiconductors. *J. Appl. Phys.* **93**, 7667-7669 (2003).
53. Perdew, J. P., Burke, K. & Ernzerhof, M. Generalized Gradient Approximation Made Simple. *Phys. Rev. Lett.* **77**, 3865-3868 (1996).
54. Hafner, J. Ab-initio simulations of materials using VASP: Density-functional theory and beyond. *J. Comput. Chem.* **29**, 2044-2078 (2008).
55. Blochl, P. E. Projector augmented-wave method. *Phys. Rev. B* **50**, 17953-17979 (1994).
56. Mosey, N. J., Liao, P. & Carter, E. A. Rotationally invariant ab initio evaluation of Coulomb and exchange parameters for DFT+U calculations. *J. Chem. Phys.* **129**, 014103 (2008).
57. Zhuang, H. L., Kent, P. R. C. & Hennig, R. G. Strong anisotropy and magnetostriction in the two-dimensional Stoner ferromagnet Fe_3GeTe_2. *Phys. Rev. B* **93**, 134407 (2016).
58. Grimme, S., Antony, J., Ehrlich, S. & Krieg, H. A consistent and accurate ab initio parametrization of density functional dispersion correction (DFT-D) for the 94 elements H-Pu. *J. Chem. Phys.* **132**, 154104 (2010).
59. Abdullahi, Y. Z., Ersan, F., Vatansever, Z. D., Aktürk, E. & Aktürk, O. Ü. Exploring the potential of MnX (S, Sb) monolayers for antiferromagnetic spintronics: A theoretical investigation. *J. Appl. Phys.* **128**, 113903 (2020).
60. Xing, J., Wang, P., Jiang, Z., Jiang, X., Wang, Y. & Zhao, J. Rational design of 2D organic magnets with giant magnetic anisotropy based on two-coordinate 5d transition metals. *APL Mater.* **8**, 071105 (2020).

Acknowledgement

This work was supported by the National Natural Science Foundation of China (11874097, 91961204, 11804044) and the Fundamental Research Funds for the Central Universities of China (DUT19LK12). We acknowledge the project of Dalian Youth Science and Technology Star (2017RQ012). The authors also acknowledge the Supercomputing Center of Dalian University of Technology for providing the computing resources.

Author contributions

X.J. supervised this study. X.J., Y.Q. and J.J.Z. conceived the idea. Q.X.L. performed the theoretical simulations. J.P.X., Z.J. and Y.G. participated in the discussion of results. X.J. and Q.X.L. drafted the manuscript. J.J.Z. edited the manuscript. All the authors contributed to the overall scientific interpretation.

Competing interests
The authors declare no competing interests.

Additional information
Supplementary Information accompanies this paper.

Correpondence and request for material should addressed to X.J. or Y.Q.

Reprint and permission information is available online at http://www.nature.com/reprints

Publisher's note Springer Nature remains neutral with regard to jurisdictional claim in piblished maps and institutional affiliations.

Supplementary Files

This is a list of supplementary files associated with this preprint. Click to download.

- SupportingInformation.docx